Journal of Organometallic Chemistry 695 (2010) 2526–2531

Contents lists available at ScienceDirect

Journal of Organometallic Chemistry

journal homepage: www.elsevier.com/locate/jorganchem

Study of optoelectronic energy bands and molecular energy levels of tris (8-hydroxyquinolinate) gallium and aluminum organometallic materials from their spectroscopic and electrochemical analysis

Fahmi Fariq Muhammad*, Ali Imran Abdul Hapip, Khaulah Sulaiman

Low Dimensional Materials Research Center, Department of Physics, Faculty of Science, University of Malaya, 50603 Kuala Lumpur, Malaysia

ARTICLE INFO

Article history:
Received 30 April 2010
Received in revised form
25 July 2010
Accepted 29 July 2010
Available online 6 August 2010

Keywords:
Cyclic voltammetry
Energy gap
Molecular energy levels
Organometallic materials
Spectroscopic analysis

ABSTRACT

For the purpose of investigating electro-molecular absorption bands, energy gaps, E_g and molecular energy levels (ionization potential, *IP* and electron affinity, *EA*) of tris (8-hydroxyquinolinate) gallium and aluminum, spectral analysis in conjunction with electrochemical measurements was carried out. UV–Vis–NIR and FTIR spectroscopic measurements were used to assign the electronic and molecular absorption bands in both of the materials. The XRD and scanning electronic microscopy (SEM) technique showed the amorphous nature. From the recorded data of cyclic voltammetry (CV) and materials absorption coefficient, HOMO, LUMO energy levels and energy gaps for Gaq3 and Alq3 were calculated. A bit smaller value of energy gap for Gaq3 (2.80 eV) compared to that of Alq3 (2.86 eV) has been ascribed to the differences in electronic configuration and coordinated bond lengths related to the central metal atom with respect to the quinolinate ligands. A higher value of HOMO energy level for the Alq3 (*IP* = 6.3 eV) revealed the need of higher potentials to oxidize its molecules comparing to that of Gaq3 (*IP* = 5.8 eV). It was observed that cationic metals have a direct effect on the physical and chemical behaviors of such organometallic materials that can be exploited to be used in tuning their properties to match the desired application in OSC and/or OLED technologies.

1. Introduction

Since the first successful use of metaloquinolate tris(8-hydroxyquinoline) aluminum (Alq3) as the electron-transport material and emitting layer in developing organic light-emitting devices (OLEDs) [1], Alq3 has attracted a lot of attention in the field of both industry and academic research. Owing to its good luminescent properties, high electron mobility, and excellent thermal stability [2], Alq3 is so far regarded as one of the most widely used material in OLED technology [3]. Recently, tris (8-hydroxyquinoline) gallium (Gaq3) as another candidate of emitting layer in OLED devices was introduced [4]. This Gaq3-based OLED, showed better performance compared to that of Alq3-based emitting layer OLED prepared under the same conditions. Triggered by such interesting phenomenon concerning Gaq3, efforts have been paid in theoretical studies to analyze the chemical bonds, molecular geometry, electronic structure [5,6] and its spectroscopic analysis at high pressure [7] to understand and improve its optical properties, respectively. Despite of having several reports on the theoretical computations [8,9] and experimental studies [10–15] by investigating the photoluminescence and optical functions of Alq3 and its derivatives [16,17], these studies are still served to understand and improve the physical behaviors of this organometallic material in OLED technology. More recently, utilization of Alq3 as buffer electron-transport layer (ELT) in organic solar cells (OSCs) between the cathode electrode and acceptor materials [18], as well as doping into their donor and/or acceptor layers [19], has opened the issue of introducing organometallic materials in OSC devices. It is thought that due to their high thermal stability and excellent electron-transport [2], introduction of these materials would be helpful to enhance the performance of OSCs, as well as to replace bathocuproin [20] and lithium fluoride [21], which are commonly used as exciton blocking or buffer layers between the cathode electrode and acceptor layers in OSCs. It was seen that using Alq3 has led to increase in both efficiency and stability of these devices [19]. The energy gaps and molecular energy band alignment between constituents are crucial to facilitate efficient electron and hole transport. Therefore, before Gaq3, Alq3 and their organometallic counterparts being applicable in OSCs, enough information concerning their energy gap and molecular energy levels is needed. As

* Corresponding author. Tel.: +60 1 23958420; fax: +60 3 79674146.
E-mail address: fahmi982@gmail.com (F.F. Muhammad).

0022-328X/$ – see front matter © 2010 Elsevier B.V. All rights reserved.
doi:10.1016/j.jorganchem.2010.07.026

far as the optical properties of Gaq3 and Alq3 are concerned, there is no practical research works on the determination of optoelectronic energy gaps and molecular energy levels of Gaq3. Along this line, the studies on Gaq3 are still limited within the scope of theoretical investigations [5,6].

Thus, there are large areas of studies that can be explored in order to understand the correlation between the optical and electrical properties of Gaq3 and Alq3. Electrochemical method [22–24] as an efficient tool can be successfully utilized to investigate the molecular energy bands, e.g., the ionization potential (*IP*) or higher occupied molecular energy level (HOMO), electron affinity (*EA*) or lower unoccupied molecular energy level (LUMO) and energy gap (E_g), which are important parameters in the performance of OSC devices. Motivated by these, the current report discusses the optoelectronic energy bands and molecular energy levels of both Gaq3 and Alq3 organometallic semiconductors, obtained via absorbance and transmittance spectroscopic measurements as well as their electrochemical analysis.

2. Materials and methods

The organometallic materials, tris (8-hydroxyquinolinate) gallium (Gaq3) and tris (8-hydroxyquinolinate) aluminum (Alq3) were purchased from Sigma–Aldrich and used without further purification. Three dimensional chemical structure view of these organometallic materials with linear molecular formula of M $(C_9H_6NO)_3$, where M = Ga or Al, and having three ligands each with a phenoxide and pyridyl side groups is shown in Fig. 1. Films of Gaq3 and Alq3 were thermally evaporated onto the pre-cleaned quartz slides by a home-made thermal evaporator under a pressure of about 10^{-4} mbar. The quartz slides were cleaned ultrasonically with Deacon® Neutracon foam solution for 15 min followed by rinsing in acetone, ethanol and distilled water for 10 min in an ultrasonic bath, respectively. Finally, the quartz slides were dried thoroughly by blowing the nitrogen gas.

For the purpose of measuring thickness of the films, transmittance spectra in the long range of 200–2500 nm were taken at room temperature by using a Jasco V-570 UV–Vis–NIR spectrophotometer. The optical absorption spectra were recorded in the wavelength range from 220 to 820 nm for the aim of determining the energy gaps. A Nicolet IS10-Thermo scientific Fourier Transform Infrared Spectrophotometer (FTIR) system was also used, the absorbance spectra recorded from 400 to 4000 cm^{-1} to analyze the molecular spectroscopic properties of the films. In addition, field emission scanning electronic microscopy (FESEM, Quanta 200F) was utilized to capture the surface images to visualize the surface morphology and structural distribution of the films. In order to figure out the molecular energy diagram and calculate the ionization potential (*IP*), HOMO and electron affinity (*EA*), LUMO molecular energy levels of both materials, electrochemical analyses using Cyclic Voltammetry (CV) measurements were carried out on MCA Microcell (ALS, Japan)/PGSTAT100 potentiostat electrochemical workstation interfaced with special auto lab CV software. The tests were done with 0.1 M solutions of the material in CH_2Cl_2 containing supporting electrolyte of tetrabutylammonium perchlorate, $(C_4H_9)_4NClO_4$ in a three-electrode cell, where indium tin oxide (ITO) plate was the working electrode, Pt wire was the counter electrode, and saturated calomel electrode (SCE) was used as the reference electrode. The concentration of Gaq3 and Alq3 in the solution was fixed to 5 mg/ml.

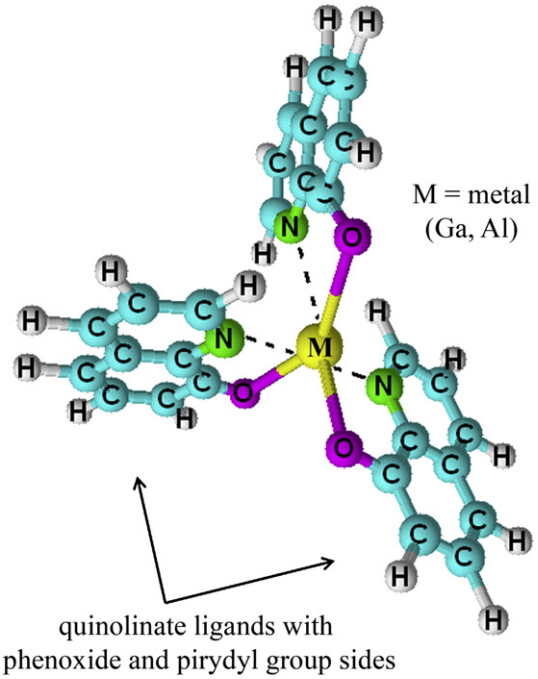

Fig. 1. The chemical structure of Mq3 (M = Ga, Al and *q* = 8-hydroxyquinolinate).

3. Results and discussion

3.1. Thickness determination

Fig. 2 shows the transmittance spectra of Gaq3 and Alq3 films. The produced fringes are due to the interference phenomena between the wave fronts created at the two interfaces (air and quartz substrate), which defines the sinusoidal behavior of the curves in the region of high transparency. Since these organometallic films exhibited a good transparency in the visible and infrared region, the envelope method [25] is a sensitive tool and thus was chosen to determine their thicknesses. To do this, the refractive index for the films was first calculated at various wavelengths along the envelope created, by fitting the transmission maxima and minima of the interference fringes, T_{max} and T_{min} respectively, using the expression [26]:

$$n = \sqrt{N + \sqrt{N^2 - S^2}} \quad (1)$$

where,

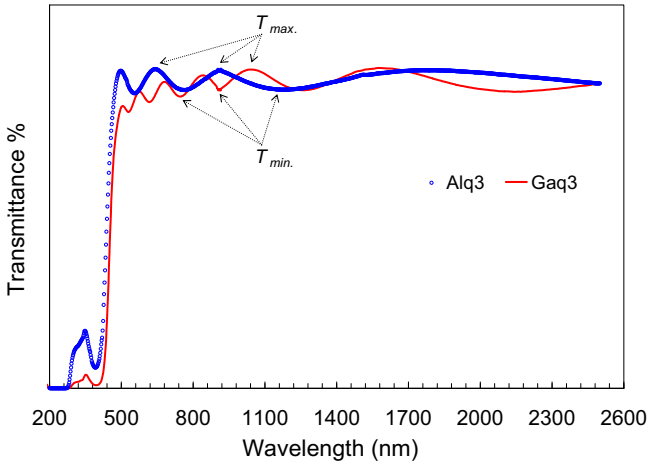

Fig. 2. Transmittance spectra of Gaq3 and Alq3 films.

$$N = 2S\left(\frac{T_{max} - T_{min}}{T_{max} \times T_{min}}\right) + \frac{S^2 + 1}{2} \quad (2)$$

and S is the refractive index of the quartz substrate, T_{max} and T_{min} are the tangents to the envelope of the transmittance, respectively. In Fig. 2, the arrows show the position of these maxima and minima along the transmission curves.

The interference maxima shown in Fig. 2 can be used to determine the optical thickness nt of the films, where t is the geometrical thickness. Successive extremes occur at wavelengths $\lambda_m$and λ_{m+1} given by the equations [27]:

$$m\lambda_m = 2n_{\lambda m}t \quad (3)$$

$$(m+1)\lambda_{m+1} = 2n_{\lambda m+1}t \quad (4)$$

where the integer m is the order of the fringes. The value of m was calculated from the fitting of nt versus λ in the range of the envelope spectra. The obtained films thickness as tabulated in Table 1 shows average thickness of about 763.5 nm for the Gaq3 and 390.9 nm for Alq3 films. A higher thickness corresponding to a larger number of interference fringes along the transmittance spectra, six to seven fringes were observed for the Gaq3 films while Alq3 films showed only three to four fringes.

3.2. Absorption bands assignment

The absorption spectra of both types of films are shown in Fig. 3. There are two clear absorption peaks, at 266 nm and 396 nm for Gaq3 films and at 262 nm and 392 nm for Alq3. Those of Alq3 were found to be close values to the ones previously reported in literature [10,11]. However, the electronic energy levels as indicated by the absorption bands appear at lower energy (higher wavelength) for Gaq3 in comparison with Alq3. This could be due to the stronger electronic effect of the coordinated gallium central metal on its quinolinate molecular orbitals as the radius of Ga^{3+} (0.62 Å) is higher than of Al^{3+} (0.53 Å) [28]. This stronger bonding results in the more compact packing bearing an increased $\pi-\pi$ orbital overlap, hence decreasing the HOMO–LUMO space [7] to produce a red shift excitation absorption (lower photon energy) in the absorption spectra of Gaq3 comparing to that of Alq3 (see Fig. 3) and a lower energy gap as we discuss it later.

The absorption band in the UV region is known as the Soret (B) band and in the visible region as Q-band. From Fig. 3, the absorption spectra for the both materials reveal two Soret bands. According to Kumar et al., the electronic transitions that are involved in the ultraviolet and visible regions in these kinds of organics are of the type $\sigma \rightarrow \sigma^*$, $n \rightarrow \pi^*$ and $\pi \rightarrow \pi^*$ [29]. It is thought that $\pi \rightarrow d$ transition is involved when strong absorption occurs near 288 nm and the absorption bands in the region of 210–275 nm, whilst the Soret band could be due to $d \rightarrow \pi^*$ transition [30]. Therefore, in the high-energy region of the Soret band at 266 nm and 262 nm for Gaq3 and Alq3, respectively, suggests the presence of a p-band associated with the central metal atoms, where the transition $p \rightarrow \pi^*$ is more prominent, i.e. the electronic transitions from 4p electronics to π^* molecular orbitals for the Gaq3 and from 3p electronics to π^* molecular orbitals for the Alq3 are allowed. As well as, the low energy bands (Q-bands), at 396 nm and 392 nm for Alq3 and Gaq3, respectively, are attributed to the $\pi \rightarrow \pi^*$ excitation between bonding and anti-bonding molecular orbitals among the quinolinate ligands [6,16].

Table 1
Measured thickness of Gaq3 and Alq3 films.

Gaq3		Alq3	
Thickness (nm)	Avg. thickness (nm)	Thickness (nm)	Avg. thickness (nm)
754.93	763.52 ± 9.0	392.11	390.90 ± 2.0
773.10		389.79	
770.67		388.82	
755.39		392.89	

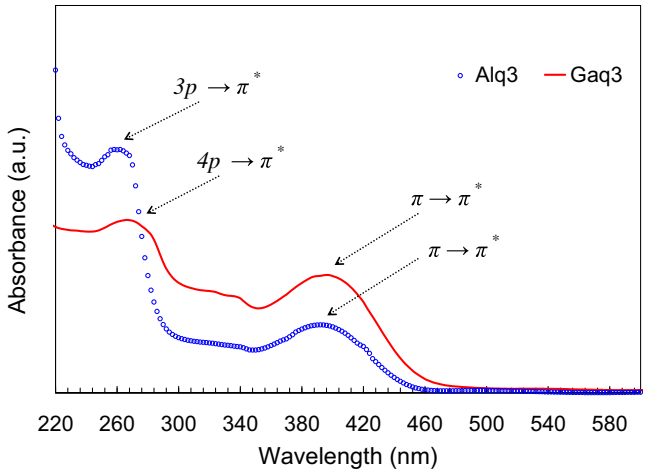

Fig. 3. Absorption spectra of Gaq3 and Alq3 films showing relatively broad electronic absorption peak.

Fig. 4 shows the recorded FTIR spectra ranging from 700 to 1800 cm^{-1} for the films of Gaq3 and Alq3. The wavenumber region shown in the spectra corresponds to the "fingerprint region" of the vibrational modes present in Gaq3 and Alq3. The same principal infrared absorption bands for Alq3 in our investigations have been previously observed by other researchers [31,32]. It can be seen that, however, the position of the principal vibration modes is relatively unchanged for both of the materials, the bands near 1460 and 1500 cm^{-1} (dashed circle in Fig. 4) show opposite molecular absorption intensity. The peak at 1500 cm^{-1} being less intense than that at 1460 cm^{-1} for Gaq3; while for Alq3 it is more intense. These bands are assigned to CC/CN stretching and CH bending of the quinolinate fragments as well as CC/CN stretching plus CH bending vibration associated with both the pyridyl and phenyl groups, respectively. The observed different IR intensities for these modes can be explained in terms of different molecular dynamics and/or coordination bond lengths that have been mentioned previously.

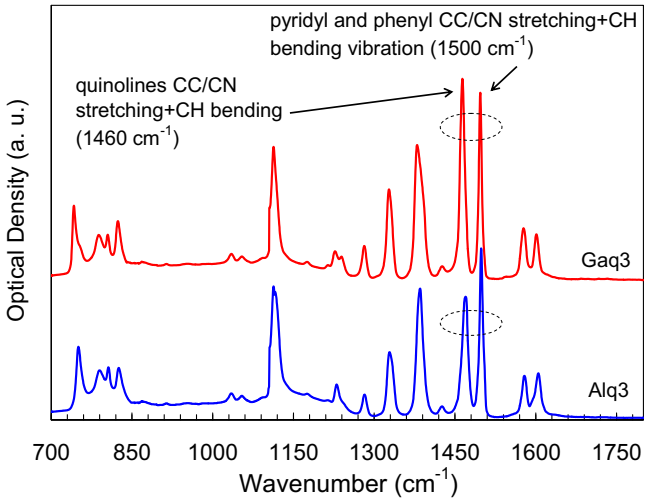

Fig. 4. FTIR spectra of the Gaq3 and Alq3 films at their fingerprint zone.

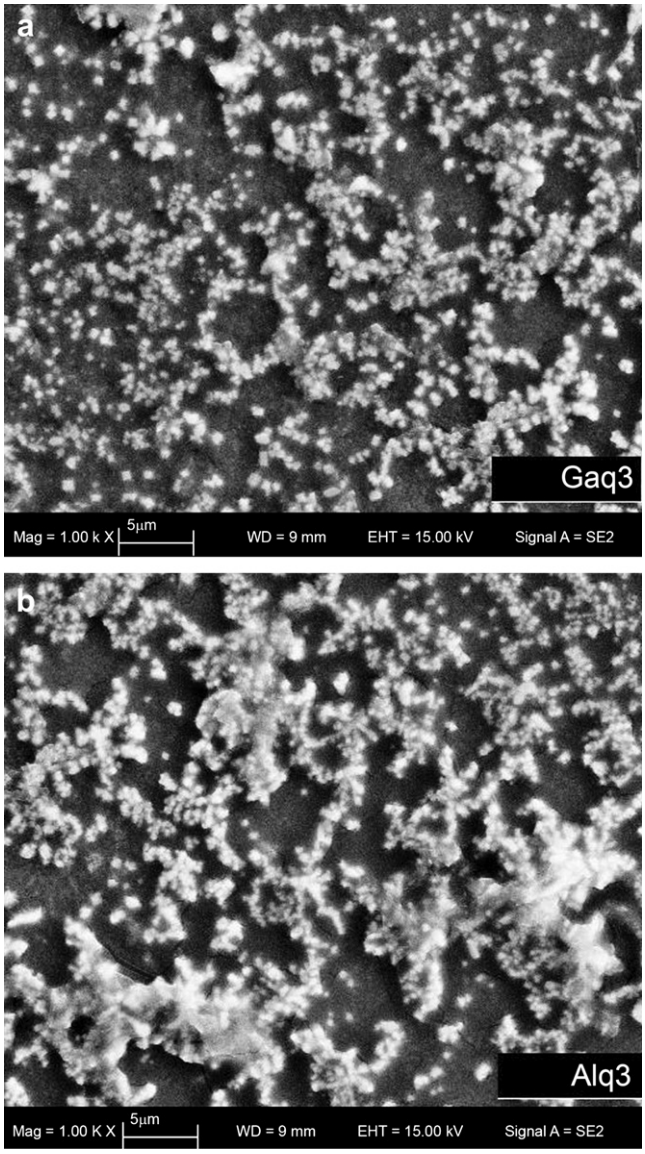

Fig. 5. FESEM surface images of Gaq3 (a) and Alq3 (b) films captured at 5 μm.

Fig. 5 shows the FESEM pictures of the surface morphology of Gaq3 and Alq3 films on quartz slides. Interestingly, the films consist of a random distribution of amorphous aggregations on the quartz surface, showing larger size in the case of Alq3 than in Gaq3. The amorphous nature of these grains was proven by X-Ray diffraction (XRD) (not shown). We assign the size differences of the Gaq3 and Alq3 grains to differences in the growth kinetics and sublimation temperatures of these materials onto the quartz substrates.

3.3. Energy gap determination

Optical absorption spectra constitute one of the most important means to determine the optical energy gap, E_g of organic and inorganic semiconductors. Optical measurements have been performed for Gaq3 and Alq3 films. The absorption coefficient (α) was calculated using the relation $\alpha = 2.303A/t$ where, A is the absorbance of the film and t its thickness. The optical energy gap of the films was then deduced by applying the Tauc relationship [33]:

$$\alpha h\nu = \alpha_o (h\nu - E_g)^n \quad (5)$$

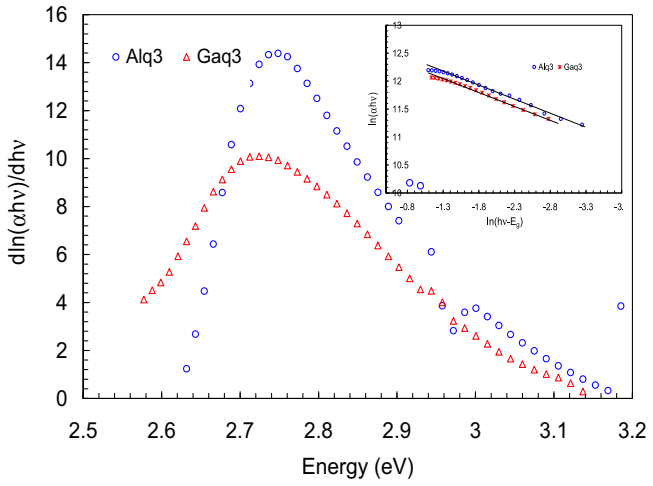

Fig. 6. Plots of $d\ln(\alpha h\nu)/dh\nu$ versus $h\nu$ for Gaq3 and Alq3 films (the inset figure, $\ln(\alpha h\nu)$ vs. $\ln(h\nu - E_g)$ were plotted to determine the value of n).

where, α_o is an energy-independent constant and E_g is the energy gap. The value of n in Eq. (5) determines the type of the absorption transition, $n = 1/2$ and 2 for direct and indirect allowed transitions, respectively. By taking natural logarithm and derivation, we can rearrange the above equation as:

$$\frac{d\ln(\alpha h\nu)}{dh\nu} = \frac{n}{h\nu - E_g} \quad (6)$$

According to Eq. (6), a peak in the curve of $d\ln(\alpha h\nu)/dh\nu$ versus $h\nu$ should be observed at a point nearly where $h\nu = E_g$. Fig. 6 shows the plot of $d\ln(\alpha h\nu)/dh\nu$ vs. $h\nu$for both types of films. The peak at a particular energy value gives approximately the value of E_g. By utilizing this initial value of E_g, graph of $\ln(\alpha h\nu)$ versus $\ln(h\nu - E_g)$ was plotted to determine the value of n. From the slope of the curves (inset of Fig. 6), $n \sim 0.5$ was determined for both Alq3 and Gaq3. Interestingly, this estimation evidences the presence of a direct gap between the intermolecular energy bands in these organometallic materials.

In order to determine the precise value of energy gap, graphs of $(\alpha h\nu)^2$ against $h\nu$ were plotted, as shown in Fig. 7. Extrapolation of this plot for $(\alpha h\nu)^2 = 0$ gives the energy gap, E_g. By exploiting this method, we assign the presence of direct allowed transition with energy gaps of 2.80 eV and 2.86 eV for Gaq3 and Alq3 films, respectively. The accuracy of these values was calculated to be ±0.01 eV. The detailed results of the calculated energy gap values in

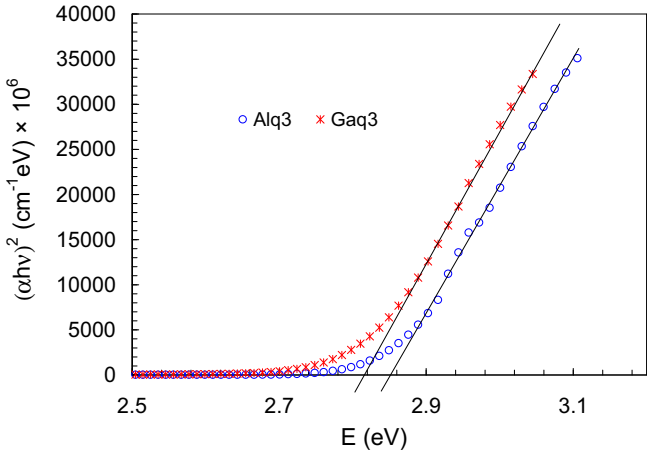

Fig. 7. Plots of $(\alpha h\nu)^2$ versus photon energy E for Gaq3 and Alq3 films.

Table 2
Determined energy gaps, E_g of Gaq3 and Alq3 films.

Gaq3		Alq3	
E_g (eV)	Avg. E_g (eV)	E_g (eV)	Avg. E_g (eV)
2.81	2.80 ± 0.01	2.85	2.86 ± 0.01
2.79		2.86	
2.80		2.86	
2.80		2.85	

several samples are shown in Table 2. The results show that the energy gap of Gaq3 is smaller than that of Alq3. This smaller energy gap for Gaq3 is thought referred to the differences in electronic configuration of the central cations, Ga^{3+} and Alq^{3+}, where the most outer electrons of Ga will occupy different arrangements and bonding lengths with respect to the atoms of phenoxide and pyridyl side groups compared with those of Al [6]. From the X-ray and theoretical simulation data [5,6,8] the only slightly longer distance for Ga–O has been proven while the other bond lengths of O–Ga–N, O–Ga–O and N–Ga–N are shorter than that of their –Al– counterpart bonds. Consequently, this originates the larger π–π intermolecular orbitals interaction and smaller E_g value for Gaq3. Another evidence to support this can be observed from the results obtained by Hernāndez and Gillin [7] upon study of hydrostatic pressure influence on these materials. It was seen that the pressure-induced intermolecular distance reduction and abrupt red shift in the absorption and photoluminescence spectra have taken place at 3.9 and 2.8 GPa for Alq3 ad Gaq3 films, respectively. This red shift was attributed to the enhancement of π–π stacking interactions as high pressure decreases the intermolecular distances and narrows the band gap energy [7]. Therefore, the lower induced pressure for Gaq3 (2.8 GPa) in compare to Alq3 (3.9 GPa) suggests the higher compressibility for Alq3 than that for Gaq3, i.e. the lower pristine π–π stacking interactions for Alq3 and higher for Gaq3. As the higher π–π orbital interaction bearing narrower energy gap, therefore; the Gaq3 shows smaller energy gap, E_g to that of Alq3 films.

3.4. Molecular energy levels and band gap diagram

Electrochemical reduction and oxidation potentials (redox) for the complexes were measured by cyclic voltammetry (CV) technique to obtain the frontier orbital energy levels and band gap diagram of Gaq3 and Alq3. Fig. 8 shows the CV curves of Gaq3 and Alq3 within the electrochemical window of CH_2Cl_2 with one-electron quasi-reversible reduction and oxidation peaks ($E^1_{1/2}$, vs. SCE). The cathodic scans corresponding to n-doping (electron migration into the materials) show well-defined irreversible peaks for Gaq3 compared to Alq3. This indicates Gaq3 possesses a higher stability than Alq3. Since the oxidation state of the central metal cations does not change [22], these redox processes are attributed to the removal or addition of electron from or to ligand-based orbitals. The onset potentials (E_{red}) of the materials were estimated by analyzing the intersection of the two slopes drawn at the falling reduction current and background current in the cyclic voltammograms (shown as inset of Fig. 8). The value of E_{red} was found to be −1.25 V and −0.86 V for Gaq3 and Alq3, respectively. It is worthy of note that the reduction peaks of Alq3 are not well resolved under normal scanning rate [34], however, they become obvious in the 1st derivative of the CV curve. For estimating the ionization potential (*IP*) and the electron affinity (*EA*) from the measured redox potentials we need to correlate the electrochemical potentials to the vacuum energy level. In order to do so, it is convenient to use the standard hydrogen electrode (platinum wire electrode) as the reference for the potential values (*E*), and then correct these potentials using the vacuum level reference.

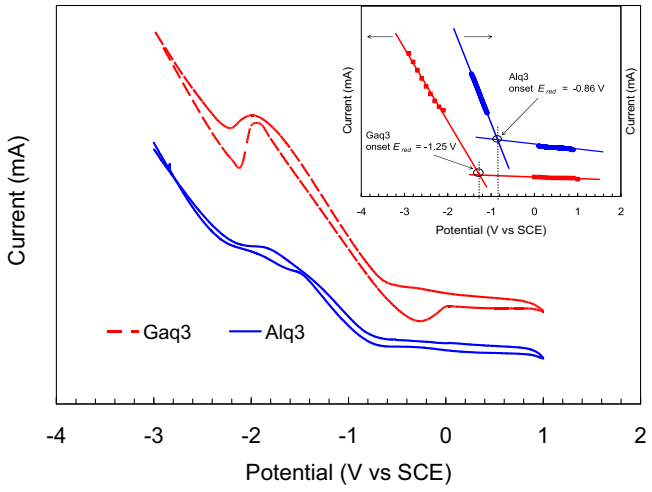

Fig. 8. Cyclic voltammograms of Gaq3 and Alq3 in CH_2Cl_2 solution.

The energy level of the standard hydrogen electrode (SHE) is found 4.5 eV below the zero vacuum energy level [35]. From this energy level and the reduction potential of the reference electrode used in the present work SCE (=0.242 V) versus SHE, a simple relation can be written which allows estimating the magnitude of electron affinity:

$$EA = [4.5 - (0.242 + |E_{red}|)]\text{eV} \quad (7)$$

As the value of energy gap equal to the magnitude differences of *IP* and *EA* ($E_g = IP - EA$), so it is possible to calculate the value of *IP* from the following equation:

$$IP = EA + E_g \quad (8)$$

The data obtained from the cyclic voltammograms of Gaq3 and Alq3 are summarized in Table 3. Lower values of *EA* (2.82 eV) and E_g (2.81 eV) for Alq3 were deduced by Shia et al. [34] previously, but unfortunately no complete information given concerning their calculations whether the potential values have been corrected using the vacuum level reference or not. What is clear, they have used platinum for both of the working and counter electrodes, while our working electrode is ITO. Nevertheless, in the current work for precise E_g calculation we have utilized Eq. (5) rather than absorbance spectra alone, which guarantee a precise determination of E_g. Therefore, by utilizing the calculated values we can construct the band structure of both materials as shown in Fig. 9. A higher value of HOMO energy level for the Alq3 reveals the need of higher potential to oxidize its molecules. Moreover, the differences in the energy levels of both organometallic materials possibly relate to the effect of central metal cations on the molecular oxidizations.

Further studies on the effect of cation sizes upon the physical and chemical behaviors of such materials will deliver a better understanding, allowing to perform a precise tuning of their optoelectronic energy gap and photo-absorption properties. Such tuning can be achieved by means of doping and/or coordination

Table 3
Estimated molecular energy levels, optoelectronic energy gap, E_g and the absorption peak bands for Alq3 and Gaq3 organometallic materials obtained from spectroscopic and electrochemical analysis data.

Material	Abs. band (nm)	HOMO (eV)	LUMO (eV)	Optoelectronic E_g (eV)
Gaq3	396, 266	5.8	3.0	2.80
Alq3	392, 262	6.3	3.4	2.86

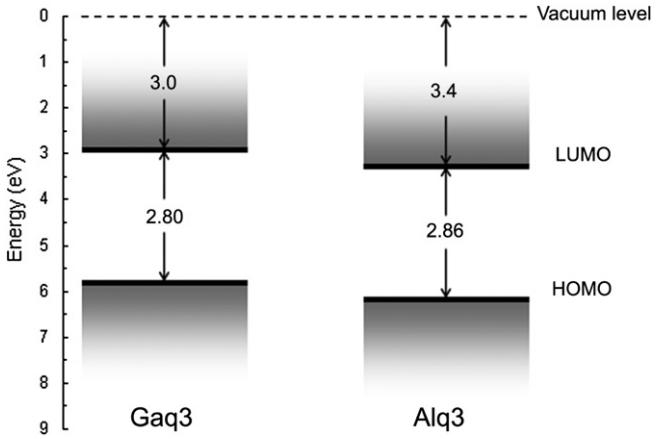

Fig. 9. Band gap and molecular energy levels diagram for Gaq3 and Alq3.

transformations, producing material derivatives to meet the desired applications in OSC and/or OLED technologies.

4. Conclusion

The absorption bands, optoelectronic energy gap and molecular energy levels (HOMO and LUMO) for Gaq3 and Alq3 have been investigated by means of spectroscopic and electrochemical analyses. The occurrence of Soret bands in the electronic absorption region of the materials is attributed to the presence of $\pi \rightarrow \pi^*$ and $p \rightarrow \pi^*$ transitions at the lower and higher absorption energy, respectively. From the molecular absorption bands using FTIR spectra, differences in molecular vibration energy have been detected such that Gaq3 showed higher CC/CN stretching plus CH bending vibration associated with both the pyridyl and phenyl groups. In addition, we have determined the optoelectronic energy gaps of 2.80 eV and 2.86 eV for Gaq3 and Alq3 films, respectively, with the accuracy of $\pm$0.01 eV. The smaller energy gap for Gaq3 has been ascribed to the differences in electronic configuration and bonding length of the Ga(III) central ion, in comparison with the Al(III) ion and relative to the bonded atoms in their quinolinate ligands. A lower value of HOMO energy level for Gaq3 has been deduced that reveals the need of smaller potentials to oxidize its molecules compared to that of Alq3. The difference in the energy levels of the two organometallic materials suggests that the central cations size, Ga^{3+} (0.62 Å) and Al^{3+} (0.53 Å) plays a major role affecting the optical and redox properties of these systems.

Acknowledgments

We thank University of Malaya for providing the research grants PS319/2009B and RG053/09AFR to support this research work. One of the authors, Fahmi Fariq Muhammad wishes to thank Ministry of Higher Education of Kurdistan Regional Government/Iraq for their awarded scholarship to pursue his PhD abroad. The authors thank Dr. I. Hernández Campo for his scientific suggestions and language editing on the paper.

References

[1] M. Ghedini, M.L. Deda, I. Aiello, A. Grisolia, Synth. Met. 138 (2003) 189–192.
[2] L. Li, B. Xu, Tetrahedron 64 (2008) 10986–10995.
[3] J.R. Lian, Y. Yuan, L. Cao, J. Zhang, H. Pang, Y. Zhou, X. Zhou, J. Lumin. 122–123 (2007) 660–662.
[4] L. Wang, X. Jiang, Zh. Zhang, S. Xu, Displays 21 (2000) 47–49.
[5] G. Gahungu, J. Zhang, J. Mol. Struct.: Theochem 755 (2005) 19–30.
[6] J. Zhang, G. Frenking, Chem. Phys. Lett. 394 (2004) 120–125.
[7] I. Hernández, W.P. Gillin, J. Phys. Chem. B 113 (2009) 14079–14086.
[8] A. Curioni, M. Boero, W. Andreoni, Chem. Phys. Lett. 294 (1998) 263–271.
[9] S. Dong, W. Wang, S. Yin, C. Li, J. Lu, Synth. Met. 159 (2009) 385–390.
[10] D.Z. Garbuzov, V. Bulovic, P.E. Burrows, S.R. Forrest, Chem. Phys. Lett. 249 (1996) 433–437.
[11] V.V.N. Ravi Kishore, A. Aziz, K.L. Narasimhan, N. Periasamy, P.S. Meenakshi, S. Wategaonkar, Synth. Met. 126 (2002) 199–205.
[12] P. Dalasinski, P. Dalasinski, Z. Łukasiak, M. Wojdyła, M. Rebarz, W. Bała, Opt. Mater 28 (2006) 98–101.
[13] A.B. Djurisic, C.Y. Kwong, W.L. Guo, T.W. Lau, E.H. Li, Z.T. Liu, H.S. Kwok, L.S.M. Lam, W.K. Chan, Thin Solid Films 416 (2002) 233–241.
[14] A. Meyers, M. Weck, Chem. Mater. 16 (2004) 1183–1188.
[15] V.K. Shukla, S. Kumar, D. Deva, Synth. Met. 156 (2006) 387–391.
[16] V.P. Barberis, J.A. Mikroyannidis, Synth. Met. 156 (2006) 865–871.
[17] J.T. Lim, C.H. Jeong, J.H. Lee, G.Y. Yeom, H.K. Jeong, S.Y. Chai, I.M. Lee, W.I. Lee, J. Organomet. Chem. 691 (2006) 2701–2707.
[18] P. Vivo, J. Jukola, M. Ojala, V. Chukharev, H. Lemmetyinen, Sol. Energy Mater. Solar Cells 92 (2008) 1416–1420.
[19] P.C. Kao, S.Y. Chu, H.H. Huang, Z.L. Tseng, Y.Ch. Chen, Thin Solid Films 517 (2009) 5301–5304.
[20] S. Yoo, W.J. Potscavage Jr., B. Domercq, S.H. Han, T.D. Li, S.C. Jones, R. Szoszkiewicz, D. Levi, E. Riedo, S.R. Marder, B. Kippelen, Solid State Electron. 51 (2007) 1367–1375.
[21] C.J. Brabec, S.E. Shaheen, C. Winder, N.S. Sariciftci, P. Denk, Appl. Phys. Lett. 80 (2002) 1288.
[22] J.W. Zhang, P.F. Yan, G.M. Li, B.Q. Liu, P. Chen, J. Organomet. Chem. 695 (2010) 1493–1498.
[23] I.S. Lee, Y.W. Kwak, D.H. Kim, Y. Cho, J. Ohshita, J. Organomet. Chem. 693 (2008) 3233–3239.
[24] G. Angulo, A. Kapturkiewicz, A. Palmaerts, L. Lutsen, T.J. Cleij, D. Vanderzande, Electrochim. Acta 54 (2009) 1584–1588.
[25] M. Caglar, Y. Caglar, S. Ilican, J. Optoelectron. Adv. Mat 8 (2006) 1410–1413.
[26] A.F. Qasrawi, Cryst. Res. Technol. 40 (2005) 610–614.
[27] E.A. Davis, N. Piggins, S.C. Bayliss, J. Phys. C Solid State Phys. 20 (1987) 415–4427.
[28] W. Kim, J.H. We, S.J. Kim, C.S. Kim, J. Appl. Phys. 101 (2007) 09M515.
[29] R. Kumar, S.A. Ali, A.K. Mahur, H.S. Virk, F. Singh, S.A. Khan, D.K. Avasthi, R. Prasad, Nucl. Instrum. Methods Phys. Res. B 266 (2008) 1788–1792.
[30] A.A.M. Farag, Opt. Laser Technol. 39 (2007) 728–732.
[31] J.Y. Koay, K.A.M. Sharif, S.A. Rahman, Thin Solid Films 517 (2009) 5298–5300.
[32] U.S. Bhansali, M.A.Q. Lopez, H. Jia, H.N. Alshareef, D.K. Cha, M.J. Kim, B.E. Gnade, Thin Solid Films 517 (2009) 5825–5829.
[33] F. Karipcin, S. Ilican, Y. Caglar, M. Caglar, B. Dede, Y. Şahin, J. Organomet. Chem. 692 (2007) 2473–2481.
[34] M.-M. Shia, J.-J. Lina, Y.-W. Shia, M. Ouyanga, M. Wanga, H.-Z. Chena, Mat. Chem. Phys. 115 (2009) 841–845.
[35] A.J. Bard, L.R. Faulkner, Electrochemical Methods Fundamentals and Applications, second ed.. John Wiley & Sons, New York, 2001.